An Introduction and Tutorial to the "McKenzie Equations" for magma migration

Marc Spiegelman[1,2], Richard Katz[1,3] and Gideon Simpson[2]

[1] Lamont-Doherty Earth Obs. of Columbia University

[2] Dept. of Applied Physics and Applied Mathematics, Columbia Univ.

[3] Dept. of Theoretical Physics and Applied Mathematics, Cambridge University

January 13, 2007

1 Introduction

Magmatism is a fundamental feature of plate boundaries and an essential process controlling the geochemical evolution of the planet. Nevertheless, the actual dynamics of melting and melt transport are often neglected in large scale models of mantle convection and lithospheric deformation. Based on discussions at the recent CIG workshop on Computational Magma Dynamics at Columbia University, it became clear that a concise set of notes/tutorial describing the most commonly used formulation for magma migration, along with a set of clear benchmark problems, is an important first step toward developing a larger community of developers and users interested in exploring magma dynamics.

Here we present a new formulation for the equations of magma migration in viscous materials as originally derived by McKenzie [1984]. We also present a set of well-understood special case problems that form a useful benchmark-suite for developing and testing new codes. In addition to providing a more readily available resource for understanding the "McKenzie Equations" we also want to emphasize that this formulation is tractable and is a natural extension of mantle convection (i.e. incompressible and compressible Stoke's Flow).

For clarity and simplicity, we only consider the equations for conservation of mass and momentum as derived in McKenzie [1984]. These equations are readily extendible with new physics such as reactive flow [e.g. Spiegelman et al., 2001], chemical transport [e.g. Spiegelman, 1996, Spiegelman and Kelemen, 2003] and consideration of grain-scale effects such as surface energy [e.g. Bercovici et al., 2001, Ricard et al., 2001, Hier-Majumder et al., 2006]. Given the uncertainties in many of the components of these macroscopic multi-phase theories, we expect the development of experimentally validated model systems to be an active and open problem [e.g. Katz et al., 2006]. Nevertheless, the equations of McKenzie [1984] are probably the best understood system at the present and a natural place to begin.

1.1 Dimensional equations for mass and momentum

A derivation for these equations is found in Appendix A of McKenzie [1984] which considers the macroscopic conservation of mass, momentum and energy for two interpenetrating continua consisting of a low-viscosity fluid in a high-viscosity deformable and permeable matrix. The approach taken is quite general and can be extended to other solid rheologies, however, as derived, the equations reduce to a system that consistently couples viscous mantle deformation (Stoke's flow) with Darcy's law for the fluid. The equations for conservation of mass and momentum for both phases can be written

$$\frac{\partial \rho_f \phi}{\partial t} + \boldsymbol{\nabla} \cdot [\rho_f \phi \mathbf{v}] = \Gamma \tag{1.1}$$

$$\frac{\partial \rho_s (1-\phi)}{\partial t} + \boldsymbol{\nabla} \cdot [\rho_s (1-\phi) \mathbf{V}] = -\Gamma \tag{1.2}$$

$$\phi(\mathbf{v} - \mathbf{V}) = -\frac{K}{\mu} [\boldsymbol{\nabla} P - \rho_f \mathbf{g}] \tag{1.3}$$

$$\boldsymbol{\nabla} P = \boldsymbol{\nabla} \cdot \left(\eta \left[\boldsymbol{\nabla} \mathbf{V} + \boldsymbol{\nabla} \mathbf{V}^T \right] \right) + \boldsymbol{\nabla} \left[\left(\zeta - \frac{2}{3} \eta \right) \boldsymbol{\nabla} \cdot \mathbf{V} \right] + \bar{\rho} \mathbf{g} \tag{1.4}$$

Where ϕ is porosity, ρ_f, ρ_s are the fluid and solid densities, $\mathbf{v}, \mathbf{V}$ are the fluid and solid velocity fields, Γ is the rate of mass transfer from solid to liquid (i.e. melting/crystallization rate), K is the permeability, μ is the melt viscosity, P is the fluid pressure and $\mathbf{g}$ is the acceleration due to gravity. Finally η, ζ are the shear and bulk viscosities of the solid and $\bar{\rho} = \rho_f \phi + \rho_s (1-\phi)$ is the mean density of the two-phase system [see Spiegelman, 1993a,b, for further discussion].

Equations (1.1) and (1.2) conserve mass for the fluid and solid individually and allow mass-transfer between the phases through Γ. Equation (1.3) is an extended form of Darcy's law governing the separation of melt from solid. This separation flux is proportional to the permeability and fluid-pressure gradients in excess of hydrostatic. Equation (1.4) governs momentum conservation of the solid phase which is modeled as a compressible, inertia-free viscous fluid.

An important feature of Eqs. (1.1)–(1.4) is that they consistently couple solid stresses and fluid pressure. The fluid pressure responds to solid deformation and gravity which drives fluid flow and changes the porosity. Variations in porosity and stress can then feed-back through the constitutive relations for the permeability and viscosity. Such feedbacks lead to a wide range of behavior including spontaneous flow localization and the development of non-linear magma waves (see below).

Constitutive Relations, Melting and Closure The principal non-linearities in this system arise from the constitutive relations for K and η, ζ. The permeability is often modeled as a simple power law (i.e. $K \propto \phi^n$ with $n \sim$ 2–5) but can be assumed to be a non-linear increasing function of the porosity. The solid shear viscosity η has been shown experimentally to be be porosity weakening [e.g. Hirth and Kohlstedt, 1995b,a, Mei et al., 2002] in addition to the usual temperature and strain-rate dependent behavior. The greatest uncertainty concerns the matrix bulk viscosity ζ which resists mechanical volume change of the solid. The bulk viscosity is an *effective* property of the two-phase aggregate and should be controlled by grain-scale processes in partially molten rocks. It is often assumed to be comparable in magnitude

to the shear viscosity but for constant solid density ρ_s, the bulk viscosity must become infinite in the limit $\phi \to 0$ as the overall system must reduce to incompressible Stoke's flow for the solid. Further work needs to be done to develop consistent constitutive relations for ζ based on experiments and upscaling techniques. For many simplified systems, both ζ and η are assumed to be constant (see below).

Finally, to close these equations requires a relationship for the mass transfer rate Γ. For a full thermodynamic description of melting, this requires additional conservation equations for energy (enthalpy and/or entropy), composition and equations of state for reactions and phase equilibria. However, many of the important benchmark problems can be implemented without melting or with simplified parameterizations of melting and we will outline those here.

2 A Better Formulation

Equations (1.1)–(1.4) provide a consistent coupling of mantle convection and Darcy's law and reduce to incompressible Stoke's flow for the solid in the "dry" limit $\phi \to 0$. To show this more clearly and to make the equations more tractable for computation, however, it is useful to eliminate the melt velocity from these equations and rewrite them in terms of porosity, pressure and the solid velocity field. Spiegelman [1993a] presents a similar decomposition for 2-D isoviscous problems, but here we extend it to general flows.

Pressure The key issue in these coupled fluid/solid problems is how to properly couple fluid pressure and solid stresses. In the original McKenzie formulation, P is the fluid pressure. While it is not explicit, this formulation also defines a solid pressure as

$$P_s = -(1/3)\mathrm{Tr}(\sigma_s) = P - \zeta \boldsymbol{\nabla} \cdot \mathbf{V} \tag{2.1}$$

Written as $P - P_s = \zeta \boldsymbol{\nabla} \cdot \mathbf{V}$, this implies that differences between the solid and fluid pressure drive volume changes of the solid matrix, e.g. the matrix will expand if the fluid pressure exceeds the solid pressure $(P > P_s)$. This usage is consistent with the derivation of Scott and Stevenson [1984, 1986].

A better formulation can be developed by recognizing that the fluid pressure balances several contributing components (e.g. Eq. 1.4) including body forces and dynamic pressures resulting from viscous deformation of the solid. In particular, it is useful to partition the fluid pressure into three components

$$P = P_l + \mathcal{P} + P^* \tag{2.2}$$

Where $P_l = \rho_s^0 g z$ is the reference background "lithostatic" pressure for constant solid density ρ_s^0, $\mathcal{P} = (\zeta - 2\eta/3)\boldsymbol{\nabla} \cdot \mathbf{V}$ is the "compaction" pressure due to expansion or compaction of the solid and P^* includes all remaining contributions to the pressure (particularly the dynamic pressure due to viscous shear of the matrix).

With these definitions and a bit of algebra (see Appendix A), we can eliminate the melt velocity **v** from the equations using the same basic manipulations as in Spiegelman [1993a] [see also Spiegelman et al., 2001, Spiegelman and Kelemen, 2003]. If we approximate ρ_f, ρ_s to be constant (but not equal), we can rewrite the equations as

$$\frac{D\phi}{Dt} = (1-\phi)\frac{\mathcal{P}}{\xi} + \Gamma/\rho_s \tag{2.3}$$

$$-\boldsymbol{\nabla}\cdot\frac{K}{\mu}\boldsymbol{\nabla}\mathcal{P}+\frac{\mathcal{P}}{\xi}=\boldsymbol{\nabla}\cdot\frac{K}{\mu}\left[\boldsymbol{\nabla}P^*+\Delta\rho\mathbf{g}\right]+\Gamma\frac{\Delta\rho}{\rho_f\rho_s} \tag{2.4}$$

$$\boldsymbol{\nabla}\cdot\mathbf{V}=\frac{\mathcal{P}}{\xi} \tag{2.5}$$

$$\boldsymbol{\nabla}P^*=\boldsymbol{\nabla}\cdot\eta\left(\boldsymbol{\nabla}\mathbf{V}+\boldsymbol{\nabla}\mathbf{V}^T\right)-\phi\Delta\rho\mathbf{g} \tag{2.6}$$

where

$$\frac{D\phi}{Dt}=\frac{\partial\phi}{\partial t}+\mathbf{V}\cdot\boldsymbol{\nabla}\phi$$

is the material derivative of porosity in the frame of the solid, $\xi=(\zeta-2\eta/3)$ and $\Delta\rho=\rho_s-\rho_f$.

Equation (2.3) is an evolution equation for porosity in a frame following the solid flow. In this frame, porosity changes are driven by the balance of physical volume changes ($\boldsymbol{\nabla}\cdot\mathbf{V}=\mathcal{P}/\xi$) and melting. Equation (2.4) is a modified Helmholtz equation for the compaction pressure $\mathcal{P}$ which reduces to Darcy flow in rigid porous media in the limit $\xi\rightarrow\infty$. This equation is responsible for much of the novel behavior in this system and has been discussed in detail in Spiegelman [1993a,b]. Equation (2.5) relates the divergence of the solid flow field to the compaction pressure, and Eq. (2.6) is Stoke's equation for the solid velocity and P^* with porosity driven buoyancy. Given $\phi,\mathcal{P},P^*$ and $\mathbf{V}$, the melt flux is reconstructed as

$$\phi\mathbf{v}=\phi\mathbf{V}-\frac{K(\phi)}{\mu}\left[\boldsymbol{\nabla}(P^*+\mathcal{P})+\Delta\rho\mathbf{g}\right] \tag{2.7}$$

All of these equations are in forms readily amenable to standard analytic and numerical techniques. Below we show that under reasonable approximations they reduce to a suite of problems that are well understood.

2.1 BoundaryConditions

Equations (2.3)–(2.6) form a coupled hyperbolic-elliptic set of equations for porosity, pressure and solid flow. To solve these problems require initial conditions and inflow conditions for the porosity and boundary conditions on pressure, solid velocity or stress. Most natural boundary conditions for the compaction pressure can be written in terms of the melt flux and tend to be Neumann conditions on $\mathcal{P}$. Specific boundary conditions are discussed for each model problem.

2.2 Scaling

These problems have been shown to have several intrinsic length and time scales that give rise to natural scalings. Given a reference porosity ϕ_0 ($\sim 0.1-1\%$). The *compaction length*

$$\delta=\sqrt{\frac{K(\phi_0)(\zeta+4\eta/3)}{\mu}} \tag{2.8}$$

is the length scale over which the compaction pressure $\mathcal{P}$ responds to variations in fluid flux [McKenzie, 1984, Spiegelman, 1993a]. Likewise the the *separation flux*

$$\phi_0 w_0=\frac{K(\phi_0)\Delta\rho g}{\mu} \tag{2.9}$$

is an estimate of the gravity driven melt flux relative to the solid.

These definitions give rise to a useful scaling where primes denote dimensionless variables

$$\begin{aligned} \mathbf{x} &= \delta \mathbf{x}' & \boldsymbol{\nabla} &= \boldsymbol{\nabla}'/\delta \\ \phi &= \phi_0 \phi' & t &= \frac{\delta}{w_0} t' \\ (\mathbf{v}, \mathbf{V}) &= w_0 (\mathbf{v}, \mathbf{V})' & (\mathcal{P}, P^*) &= \Delta\rho g \delta (\mathcal{P}, P^*) \\ K &= K(\phi_0) K' & \Gamma &= \frac{\rho_s \phi_0 w_0}{\delta} \Gamma' \\ \xi &= (\zeta_0 + 4\eta_0/3) \xi' & \eta &= \phi_0 (\zeta_0 + 4\eta_0/3) \eta' \end{aligned} \tag{2.10}$$

Substituting into Eqs. (2.3)–(2.7) and dropping primes yields the dimensionless equations

$$\frac{D\phi}{Dt} = (1 - \phi_0 \phi) \frac{\mathcal{P}}{\xi} + \Gamma \tag{2.11}$$

$$-\boldsymbol{\nabla} \cdot K \boldsymbol{\nabla} \mathcal{P} + \frac{\mathcal{P}}{\xi} = \boldsymbol{\nabla} \cdot K \left[\boldsymbol{\nabla} P^* + \hat{\mathbf{g}} \right] + \Gamma \frac{\Delta\rho}{\rho_f} \tag{2.12}$$

$$\boldsymbol{\nabla} \cdot \mathbf{V} = \phi_0 \frac{\mathcal{P}}{\xi} \tag{2.13}$$

$$\boldsymbol{\nabla} P^* = \boldsymbol{\nabla} \cdot \eta \left(\boldsymbol{\nabla} \mathbf{V} + \boldsymbol{\nabla} \mathbf{V}^T \right) - \phi_0 \phi \hat{\mathbf{g}} \tag{2.14}$$

where $\hat{\mathbf{g}}$ is a unit vector in the direction of gravity. In addition, for a power-law permeability, the scaled permeability is $K = \phi^n$.

3 Special Cases and Benchmark problems

Equations (2.11)–(2.14) are probably best understood through a systematic series of approximate problems that form a useful benchmark suite for developing codes. Here we present six problems of increasing complexity that have been developed and discussed in detail in the literature.

3.1 Zero porosity, no melting

In the limit $\phi = 0$ with no melting, these equations must reduce to those for incompressible Stoke's flow of the solid. Letting $\phi = K = \Gamma = 0$ and assuming $\lim_{\phi \to 0} \xi = \infty$, Eqs. (2.11)–(2.12) vanish identically and Eqs. (2.13)–(2.14) become

$$\boldsymbol{\nabla} \cdot \mathbf{V} = 0 \tag{3.1}$$

$$\boldsymbol{\nabla} P^* = \boldsymbol{\nabla} \cdot \eta \left(\boldsymbol{\nabla} \mathbf{V} + \boldsymbol{\nabla} \mathbf{V}^T \right) \tag{3.2}$$

as expected. As written, these equations are driven entirely by boundary conditions for solid velocity or stress, however, other sources of buoyancy could be included in the gravitational term. We suggest that a more general variable viscosity Stoke's solver benchmark suite be implemented as part of CIG. Accurate solutions (including accurate pressures) of Stokes are essential for solving mantle convection, long-term lithospheric/crustal deformation and magmadynamics.

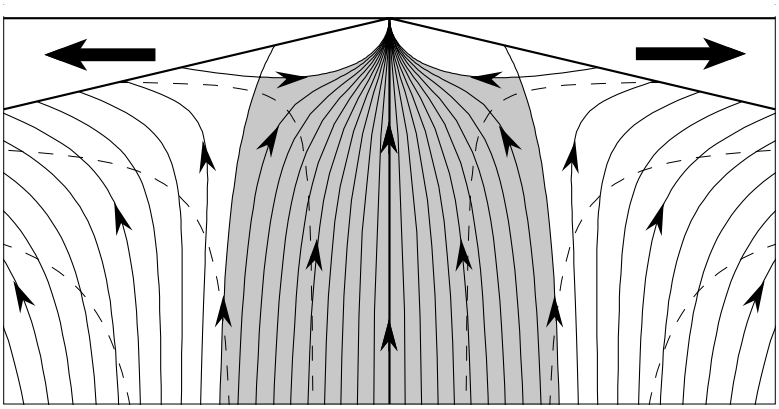

Figure 1: Melt and solid flow fields for the special case of constant porosity, constant viscosity and no melting (Section 3.3). The solid flow (dashed lines) is given by the corner flow solution [Batchelor, 1967] and the melt stream function calculated from Spiegelman and McKenzie [1987]. In general, any iso-viscous solid flow field that generates a non-constant vorticity can develop pressure gradients that affect the flow of melt. In this case, the pressure is actually singular at the corner.

3.2 Zero Permeability, no melting

A closely related problem allows for non-zero porosity but assumes the matrix is *impermeable* with $K = 0$. Again assuming that there is no melting ($\Gamma = 0$), the equations become

$$\frac{D\phi}{Dt} = 0 \tag{3.3}$$

$$\frac{\mathcal{P}}{\xi} = 0 \tag{3.4}$$

$$\boldsymbol{\nabla} \cdot \mathbf{V} = 0 \tag{3.5}$$

$$\boldsymbol{\nabla} P^* = \boldsymbol{\nabla} \cdot \eta \left(\boldsymbol{\nabla}\mathbf{V} + \boldsymbol{\nabla}\mathbf{V}^T \right) - \phi_0 \phi \hat{\mathbf{g}} \tag{3.6}$$

which describe incompressible Stoke's flow for the solid (with buoyancy terms) with passive advection of any initial porosity field. The problem, as stated, is not terribly interesting but is a useful test for any incompressible flow solver and *non-diffusive* advection scheme.

3.3 Constant porosity, iso-viscous solid, no-melting

A more interesting problem arises from the case of constant porosity $\phi = 1$, *constant* shear and bulk viscosities and no-melting [e.g. Spiegelman and McKenzie, 1987, Phipps Morgan, 1987, Spiegelman, 1993a]. The equations again reduce to incompressible Stoke's flow for the solid,

however, dynamic pressure gradients $\boldsymbol{\nabla} P^*$ are available to drive fluid flow. For dimensionless variables $\phi = 1$ $K = 1$, η, ξ constant and $\Gamma = 0$, Eqs. (2.11–2.14) reduce to

$$\boldsymbol{\nabla} \cdot \mathbf{V} = 0 \tag{3.7}$$

$$\boldsymbol{\nabla} P^* = \eta \nabla^2 \mathbf{V} - \phi_0 \mathbf{k} \tag{3.8}$$

and Eqs. (2.11)–(2.12) vanish identically. In particular Eq. (2.12) becomes

$$-\nabla^2 \mathcal{P} + \mathcal{P}/\xi = 0 \tag{3.9}$$

which for $\mathcal{P} = 0$ on the boundary of the domain implies $\mathcal{P} = 0$ everywhere in the interior. For this problem, the only pertinent boundary conditions are for Stoke's equation. The melt velocity is entirely determined by $\mathbf{V}$ and P^*.

$$\mathbf{v} = \mathbf{V} - \frac{K}{\phi_0 \mu} \left[\boldsymbol{\nabla} P^* - \hat{\mathbf{g}} \right] \tag{3.10}$$

This problem was used by Spiegelman and McKenzie [1987] and Phipps Morgan [1987] for analytic models of melt flow beneath mid-ocean ridges and island arcs where melt focusing is driven by dynamic pressure gradients due to corner flow. Figure 1 shows streamlines for both solid and melt for a ridge related problem in Spiegelman and McKenzie [1987]. This problem also provides an excellent test for pressure fields produced by incompressible solvers.

3.4 Magmatic Solitary Waves: Constant shear-viscosity, small porosity limit, no Solid Shear, no melting

Since the general equations were derived, they have been known to support non-linear dispersive porosity waves in all dimensions [e.g. Scott and Stevenson, 1984, Scott et al., 1986, Scott and Stevenson, 1986, Richter and McKenzie, 1984, Barcilon and Richter, 1986, Barcilon and Lovera, 1989]. The wave behavior is a natural consequence of the ability for the matrix to dilate or compact in response to variations in melt flux. This behavior is most readily demonstrated from solving Eqs. (2.11)–(2.14) in the limit of small porosity ($\phi_0 << 1$) with η constant, $\xi = 1$ $\Gamma = 0$. Let $K = \phi^n$ and equations reduce to

$$\frac{D\phi}{Dt} = \mathcal{P} \tag{3.11}$$

$$-\boldsymbol{\nabla} \cdot \phi^n \boldsymbol{\nabla} \mathcal{P} + \mathcal{P} = \boldsymbol{\nabla} \cdot \phi^n \hat{\mathbf{g}} \tag{3.12}$$

For constant shear viscosity, the compressible and incompressible components of the solid velocity $\mathbf{V}$ decouple. Equations (3.11)–(3.12) are valid in the limit that the solid is nearly static except for a small compressible component of order ϕ_0 (alternatively that the solid flow field can be written exclusively in terms of a scalar potential $\mathbf{V} = \boldsymbol{\nabla} \mathcal{U}$). These equations admit non-linear solitary waves in 1,2 and 3 dimensions (Figure 2) that propagate over a uniform porosity background with fixed form and constant speed. For the 1-D waves, analytic solutions exist for all integer n with perhaps the clearest derivation in Barcilon and Richter [1986] for $n = 3$ [see also Spiegelman, 1993b]. For higher dimensional waves, Barcilon and Lovera

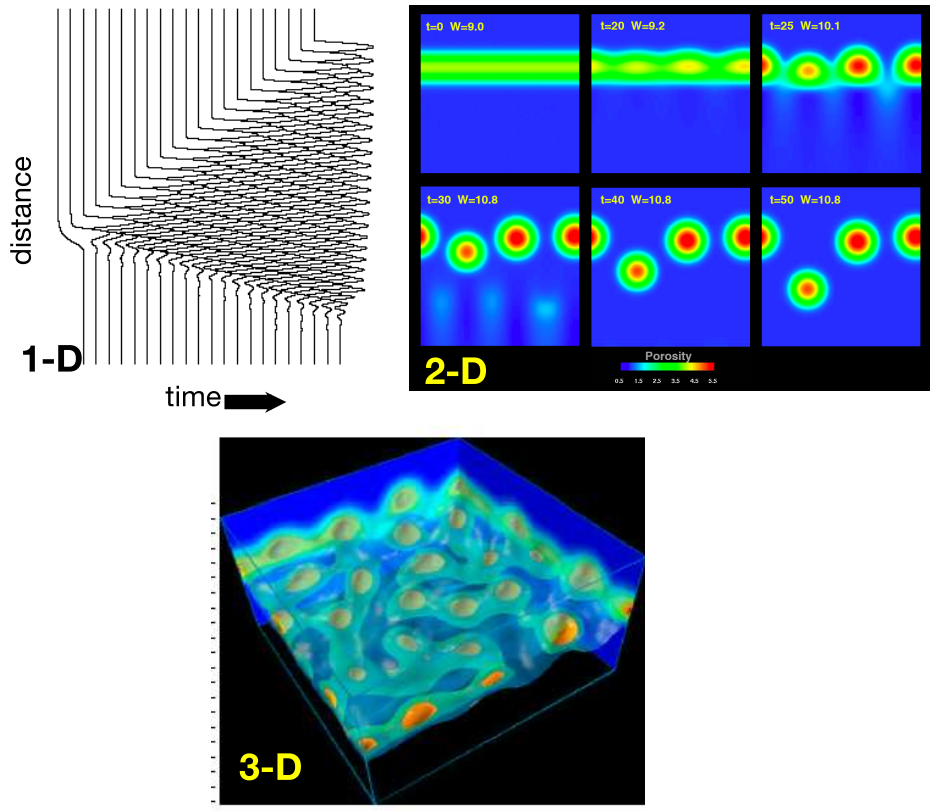

Figure 2: Solitary Waves in 1-,2- and 3-D. 1-D solutions from Spiegelman [1993a,b]. 2- and 3-D solutions from Wiggins and Spiegelman [1995].

[1989] rewrite the problem as an integro-differential equation and describe a shooting method for calculating wave profiles. This method which was used in Wiggins and Spiegelman [1995] to calculate initial conditions. More recently, however, Simpson (in prep.) has developed a more robust spectral collocation method based on Sinc Methods [e.g. Lund and Bowers, 1992, Stenger, 1993, 2000]. This approach can calculate highly accurate solitary wave profiles in all dimensions, that provide excellent tests for numerical codes. Given a single solitary wave of the appropriate dimension, it should propagate with unchanging form and constant phase velocity. Any other behavior is an artifact of the numerical method. Matlab code for Simpsons solitary wave generators as well as several PETSc based solitary wave codes with periodic boundary conditions will be made available through the CIG web-site.

3.5 Magmatic Shear Bands: Variable shear viscosity, no melting, no buoyancy

Solitary waves develop from obstructions in melt flux on scales much larger than the compaction length. However, porosity structures can also form at scales smaller than the compaction length by a range of localization phenomena including reactive fluid flow [e.g. Spiegelman et al., 2001] and mechanical shear in a matrix with variable shear viscosity. This latter

mechanism is explored in detail in Katz et al. [2006] to explain the observations of low-angle melt-rich bands observed in shear deformation experiments [e.g. Zimmerman et al., 1999, Holtzman et al., 2003b,a]. The system of model equations can be derived from Eqs. (2.11)–(2.14) by neglecting melting and buoyancy ($\Gamma = 0$, $\hat{\mathbf{g}} = 0$) and letting viscosity be a function of porosity and strainrate ($\eta, \xi = f(\phi, \mathbf{V})$). The dimensionless equations become

$$\frac{D\phi}{Dt} = (1 - \phi_0\phi)\mathcal{P}/\xi \tag{3.13}$$

$$-\boldsymbol{\nabla}\cdot K\boldsymbol{\nabla}\mathcal{P} + \mathcal{P}/\xi = \boldsymbol{\nabla}\cdot K\boldsymbol{\nabla}P^* \tag{3.14}$$

$$\boldsymbol{\nabla}\cdot\mathbf{V} = \phi_0\mathcal{P}/\xi \tag{3.15}$$

$$\boldsymbol{\nabla}P^* = \boldsymbol{\nabla}\cdot\eta\left(\boldsymbol{\nabla}\mathbf{V} + \boldsymbol{\nabla}\mathbf{V}^T\right) \tag{3.16}$$

When the shear viscosity is only porosity weakening ($\eta = f(\phi)\ f'(\phi) < 0$) melt localization has been shown to develop in pure and simple shears in an orientiation consistent with the fastest opening direction [Stevenson, 1989, Spiegelman, 2003]. Recently Katz et al. [2006] presented full calculations for porosity and strain rate dependent shear viscosity using

$$\eta(\phi, \dot{\epsilon}) = \eta_0 \mathrm{e}^{\alpha(\phi-\phi_0)}\dot{\epsilon}_{II}^{\frac{1-n}{n}} \tag{3.17}$$

where η_0 is the shear viscosity at reference porosity ϕ_0 and strain rate. $\alpha = -28 \pm 3$ is an experimentally derived porosity-weakening coefficient [Hirth and Kohlstedt, 1995b,a, Mei et al., 2002], $\dot{\epsilon}_{II}$ is the second invariant of the incompressible component of the strain rate tensor, and n defines the power-law dependence of viscosity on stress. This viscosity is Newtonian when $n = 1$ and is a standard non-Newtonian power-law viscosity when $n > 1$ and $\phi = 0$.

Boundary Conditions The domain for this problem is periodic in x. On the boundary, w and W are both equal to zero. Then, since $\phi(w - W) = \frac{k_\phi}{\mu}\frac{dP}{dz}$, the permeability on the boundary should be zero, making the pressure in the buffer cells irrelevant to the rest of the calculations. Figure 3 shows comparison of experimental results and numerical simulations for this problem.

3.6 2 and 3-D ridge models with forced adiabatic melting

The final benchmark problem should be a 2 (and or 3-D) ridge calculation such as given in [Scott and Stevenson, 1989, Spiegelman, 1996] for the full solution of Eqs. (2.11)–(2.14) with forced adiabatic melting

$$\Gamma = \rho_s W\frac{dF}{dz} \tag{3.18}$$

where W is the solid upwelling velocity and $F(z)$ is an imposed "melting function" which describes the degree of melting expected as a function of height above the solidus (and would be roughly the porosity if the melt did not separate from the solid). Figure 4 shows some solutions from Spiegelman [1996] used to explore the chemical consequences of different melt and solid flow geometries. In the spirit of the Subduction modeling benchmark (www.geo.lsa.umich.edu/∼keken/subduction/benchmark.html/) we suggest that the magma-dynamics community, in concert with organizations such as RIDGE2000 confer to develop a mutually aggreed upon set of test problems for ridge modeling.

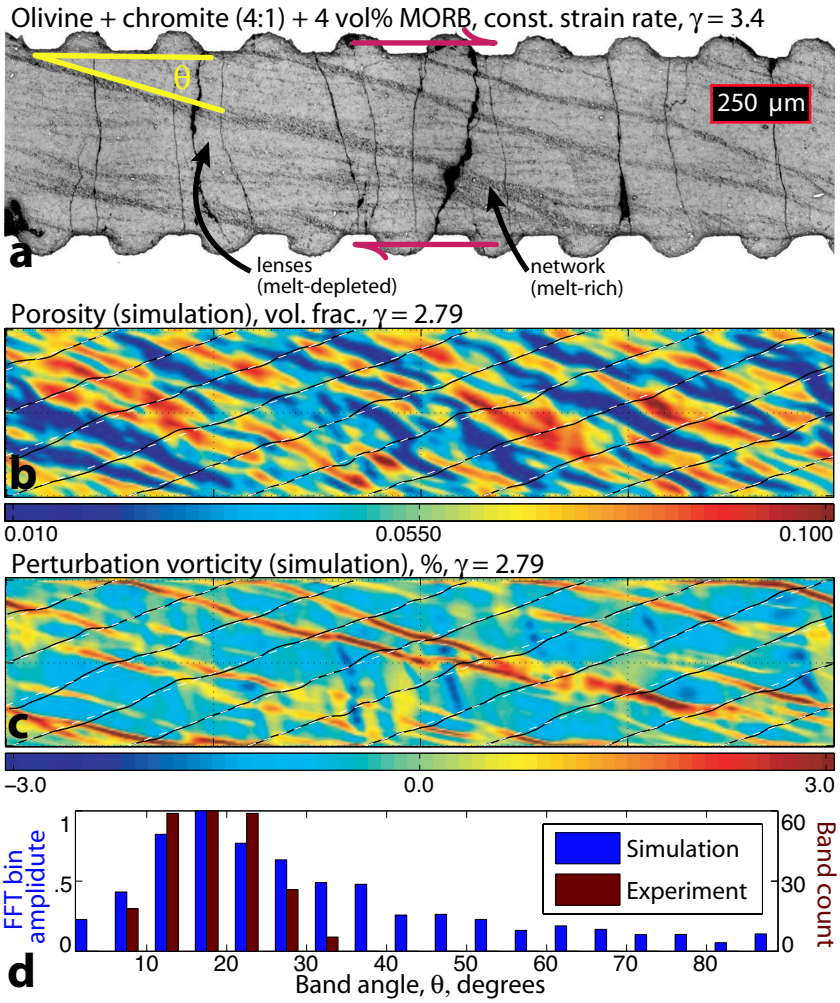

Figure 3: Figure 1 from Katz et al. [2006] comparing numerical calculations of shear induced melt localization to experiments

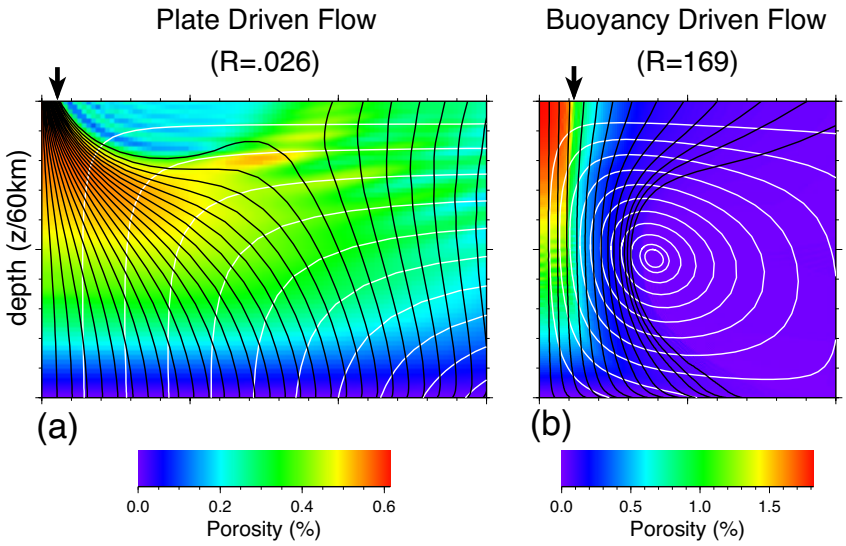

Figure 4: Example 2-D solutions for the flow of melt and solid beneath a mid-ocean ridge assuming constant shear viscosity and a linear melting function $F(z) = F_{max}/d$. A description of these calculations can be found in Spiegelman [1996]. Both solutions show half of a ridge calculation where black lines are melt flowlines, white curves are solid flow and the color scale denotes porosity. Both calculations can be described by a porosity buoyancy number R that reflects the contribution of buoyancy driven flow to plate drive flow. (a) The solid flow field is driven primarily by the boundary conditions of plate spreading. High viscosity solid develops large pressure gradients ala Spiegelman and McKenzie [1987] that focus melt to the ridge axis. (b) For lower shear viscosity, buoyancy dominates narrowing the area of upwelling. Chemically these two flow fields are distinct, however, considerably more work needs to be done to investigate the behavior of these systems in problems with porosity, temperature and strain-rate dependent solid viscosity.

References

V. Barcilon and O. Lovera. Solitary waves in magma dynamics. *J. Fluid Mech.*, 204:121–133, 1989.

V. Barcilon and F. M. Richter. Non-linear waves in compacting media. *J. Fluid Mech.*, 164: 429–448, 1986.

G. K. Batchelor. *An Introduction to Fluid Dynamics*. Cambridge Univ Press, Cambridge, 1967.

D. Bercovici, Y. Ricard, and G. Schubert. A two-phase model for compaction and damage 1. general theory. *J. Geophys. Res.-Solid Earth*, 106(B5):8887–8906, 2001.

S. Hier-Majumder, Y. Ricard, and D. Bercovici. Role of grain boundaries in magma migration and storage. *Earth Planet. Sci. Lett.*, 248(3-4):735–749, 2006.

G. Hirth and D. L. Kohlstedt. Experimental constraints on the dynamics of the partially molten upper mantle 2. deformation in the dislocation creep regime. *J. Geophys. Res.*, 100(8): 15441–15052, Aug 1995a.

G. Hirth and D. L. Kohlstedt. Experimental constraints on the dynamics of the partially molten upper mantle: Deformation in the diffusion creep regime. *J. Geophys. Res.*, 100(2):1981–2002, Feb 1995b.

B. K. Holtzman, N. J. Groebner, M. E. Zimmerman, S. B. Ginsberg, and D. L. Kohlstedt. Stress-driven melt segregation in partially molten rocks. *Geochem. Geophys. Geosyst.*, 4, 2003a. Art. No. 8607.

B. K. Holtzman, D. L. Kohlstedt, M. Zimmerman, F. Heidelbach, T. Hiraga, and J. Hustoft. Melt segregation and strain partitioning: Implications for seismic anisotropy and mantle flow. *Science*, 301(5637):1227–1230, 2003b.

R. Katz, M. Spiegelman, and B. Holtzman. The dynamics of melt and shear localization in partially molten aggregates. *Nature*, 442:676–679, 2006. doi:10.1038/nature05039.

J. Lund and K. L. Bowers. *Sinc Methods for Quadrature and Differential Equations*. SIAM, 1992.

D. McKenzie. The generation and compaction of partially molten rock. *J. Petrol.*, 25:713–765, 1984.

S. Mei, W. Bai, T. Hiraga, and D. Kohlstedt. Influence of melt on the creep behavior of olivine-basalt aggregates under hydrous conditions. *Earth Planet. Sci. Lett.*, 201:491–507, 2002.

J. Phipps Morgan. Melt migration beneath mid-ocean spreading centers. *Geophys. Res. Lett.*, 14:1238–1241, 1987.

Y. Ricard, D. Bercovici, and G. Schubert. A two-phase model for compaction and damage 2. applications to compaction, deformation, and the role of interfacial surface tension. *J. Geophys. Res.-Solid Earth*, 106(B5):8907–8924, 2001.

F. M. Richter and D. McKenzie. Dynamical models for melt segregation from a deformable matrix. *J. Geol.*, 92:729–740, 1984.

D. R. Scott and D. Stevenson. Magma solitons. *Geophys. Res. Lett.*, 11:1161–1164, 1984.

D. R. Scott and D. Stevenson. Magma ascent by porous flow. *J. Geophys. Res.*, 91:9283–9296, 1986.

D. R. Scott, D. Stevenson, and J. Whitehead. Observations of solitary waves in a deformable pipe. *Nature*, 319:759–761, 1986.

D. R. Scott and D. J. Stevenson. A self-consistent model of melting, magma migration and buoyancy-driven circulation beneath mid-ocean ridges. *J. Geophys. Res.*, 94:2973–2988, 1989.

M. Spiegelman. Flow in deformable porous media. part 1. Simple analysis. *J. Fluid Mech.*, 247:17–38, 1993a.

M. Spiegelman. Flow in deformable porous media. part 2. Numerical analysis—The relationship between shock waves and solitary waves. *J. Fluid Mech.*, 247:39–63, 1993b.

M. Spiegelman. Geochemical consequences of melt transport in 2-D: The sensitivity of trace elements to mantle dynamics. *Earth Planet. Sci. Lett.*, 139:115–132, 1996.

M. Spiegelman. Linear analysis of melt band formation by simple shear. *Geochem. Geophys. Geosyst.*, 4(9), 2003. article 8615, doi:10.1029/2002GC000499.

M. Spiegelman and P. B. Kelemen. Extreme chemical variability as a consequence of channelized melt transport. *Geochem. Geophys. Geosyst.*, 4(7), 2003. article 1055, doi:10.1029/2002GC000336.

M. Spiegelman, P. B. Kelemen, and E. Aharonov. Causes and consequences of flow organization during melt transport: The reaction infiltration instability in compactible media. *J. Geophys. Res.*, 106(B2):2061–2077, 2001. www.ldeo.columbia.edu/∼mspieg/SolFlow/.

M. Spiegelman and D. McKenzie. Simple 2-D models for melt extraction at mid-ocean ridges and island arcs. *Earth Planet. Sci. Lett.*, 83:137–152, 1987.

F. Stenger. *Numerical Methods Based on Sinc and Analytic Functions*. Springer, 1993.

F. Stenger. Summary of sinc numerical methods. *Jour. Computational and App. Math.*, 121: 379–240, 2000.

D. J. Stevenson. Spontaneous small-scale melt segregation in partial melts undergoing deformation. *Geophys. Res. Lett.*, 16(9):1067–1070, 1989.

C. Wiggins and M. Spiegelman. Magma migration and magmatic solitary waves in 3-D. *Geophys. Res. Lett.*, 22(10):1289–1292, May 15 1995.

M. E. Zimmerman, S. Q. Zhang, D. L. Kohlstedt, and S. Karato. Melt distribution in mantle rocks deformed in shear. *Geophys. Res. Lett.*, 26(10):1505–1508, 1999.

A A Detailed Derivation of the Equations in Pressure Form

The basic manipulations to derive Eqs. (2.3)–(2.6) from Eqs. (1.1)–(1.4) are straightforward and closely follow that given in Spiegelman [1993a]. We reproduce them here for completeness.

To begin, we assume that ρ_f, ρ_f are constant but not equal (i.e. the two phases are individually incompressible…this assumption can be relaxed fairly easily). We also use Eq. (2.2) as

$$P = \rho_s g z + \mathcal{P} + P^* \tag{A.1}$$

where $\mathcal{P} = (\zeta - 2\eta/3)\boldsymbol{\nabla}\cdot\mathbf{V} = \xi\boldsymbol{\nabla}\cdot\mathbf{V}$. Alternatively we can define the volumetric expansion/compaction of the solid matrix as

$$\boldsymbol{\nabla}\cdot\mathbf{V} = \frac{\mathcal{P}}{\xi} \tag{A.2}$$

Equation 2.3 With these definitions and assumptions, Eq. (2.3) is simply the expansion of Eq. (1.2)

$$\frac{\partial\phi}{\partial t} + \mathbf{V}\cdot\boldsymbol{\nabla}\phi = (1-\phi)\boldsymbol{\nabla}\cdot\mathbf{V} + \Gamma/\rho_s \tag{A.3}$$

with Eq. (A.2) substituted for $\boldsymbol{\nabla}\cdot\mathbf{V}$.

Equation (2.4) To derive Eq. 2.4, first expand Eqs. (1.1) and (1.2) as

$$\frac{\partial\phi}{\partial t} + \boldsymbol{\nabla}\cdot[\phi\mathbf{v}] = \Gamma/\rho_f \tag{A.4}$$

$$-\frac{\partial\phi}{\partial t} + \boldsymbol{\nabla}\cdot[(1-\phi)\mathbf{V}] = -\Gamma/\rho_s \tag{A.5}$$

and add to yield an equation for volume balance

$$\boldsymbol{\nabla}\cdot\mathbf{V} = -\boldsymbol{\nabla}\cdot\phi(\mathbf{v}-\mathbf{V}) + \Gamma\frac{\Delta\rho}{\rho_f\rho_s} \tag{A.6}$$

where $\Delta\rho = \rho_s - \rho_f$. Substituting Eqs. (1.3), (A.1) and (A.2 into Eq. (A.6) yields

$$\frac{\mathcal{P}}{\xi} = \boldsymbol{\nabla}\cdot\frac{K}{\mu}\left[\boldsymbol{\nabla}P^* + \boldsymbol{\nabla}\mathcal{P} + \Delta\rho\mathbf{g}\right] + \Gamma\frac{\Delta\rho}{\rho_f\rho_s} \tag{A.7}$$

which after trivial rearrangement yields Eq. (2.4).

Equation (2.5) Equation (2.5) is simply Eq. (A.2) which follows directly from the definition of $\mathcal{P}$

Equation (2.6) Equation (2.6) follows from substituting Eq. (A.1) into Eq. (1.4) and cancelling the terms involving $\mathcal{P}$ (and noting that $\bar{\rho} - \rho_s = \phi\Delta\rho$).